Istituto Nazionale di Fisica nucleare
INFN
Laboratori Nazionali di Legnaro
LNL

INFN
Istituto Nazionale
di Fisica Nucleare
Laboratori Nazionali di Legnaro

The SPES-BNCT project: Current status of the accelerator-driven thermal neutron facility Monte Carlo modeling

---

Activities performed in the framework of SPES-BNCT project

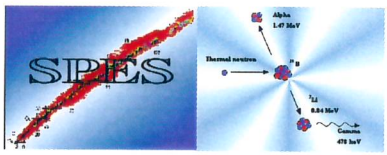

The SPES-BNCT project

INFN-LNL-219(2007)

César Ceballos Sánchez[1,2]
Juan Esposito[1]

1 INFN Laboratori Nazionali di Legnaro.
2 Centro de Aplicaciones Tecnlógicas y Desarrollo Nuclear (CEADEN), Havana, Cuba.

The SPES-BNCT project: Current status of the accelerator-driven thermal neutron facility Monte Carlo modeling

César Ceballos Sánchez[1,2], Juan Esposito[2],

1 INFN Laboratori Nazionali di Legnaro.
2 Centro de Aplicaciones Tecnlógicas y Desarrollo Nuclear (CEADEN), Havana, Cuba.

Contents.

The SPES-BNCT project: Current status of the accelerator-driven thermal neutron facility Monte Carlo modeling

César Ceballos Sánchez[1,2], Juan Esposito[2],

1 INFN Laboratori Nazionali di Legnaro.
2 Centro de Aplicaciones Tecnlógicas y Desarrollo Nuclear (CEADEN), Havana, Cuba.

I. INTRODUCTION

The SPES-BNCT project at LNL[1] is intended to perform Boron Neutron Capture Therapy (BNCT) experimental treatments on skin melanoma tumors, using a light particle accelerator as primary neutron source.

This project is part of a larger project named SPES (Study and Production of Exotic Species), currently under way at LNL, which will allow a frontier program both in nuclear and interdisciplinary physics. Other possible experimental applications, using the relatively intense neutron source which will be available may be concerned, ranging from activation analyses, up to solid state and radiobiology investigations.

The BNCT technique was first proposed by Gordon Locker[2] in 1936 and consists on tagging the cancerous cells with ^{10}B and then irradiating the tumor bulk with thermal neutrons. The resulting ^{11}B unstable nuclei breaks into ^{7}Li (0.84 MeV) + ^{4}He (1.47 MeV) fragments which release their energy within the cell dimensions causing apoptosis. In 94 % of the cases the resulting ^{7}Li nuclei remains excited so it emits a gamma ray (0.48 MeV). The $^{10}B(n,\alpha)^{7}Li$ reaction has a cross section σ=3840 b for thermal neutrons (0.025 eV).

The SPES-BNCT project will exploit the intense proton beam provided by the RFQ currently under construction at LNL in the framework of TRASCO (TRAsmutazione SCOrie) program for nuclear waste transmutation of long live actimides. This proton beam (30mA, 5MeV), will be used to yield a neutron source using the $^{9}Be(p,xn)$ nuclear reactions.

The installation of proton source TRIPS (**TRARSCO** **I**ntense **P**roton **S**ource), moved from LNS labs, was completed in late 2005 and began to extract the first beam in mid 2006.[3] On the other hand, the remaining four out of six modules of RFQ, which acts as DTL driver, are under an advanced construction stage. The TRIPS ion source and the RFQ installed at LNL will moreover represent a unique facility, able to deliver a 30 mA, 5 MeV beam, which will be used as a standalone system, as well.

Figure I.1 shows a schematic representation of the neutron production process. It can be seen the TRIPS proton source (**S**) that was setup and tested on December 2006 and generates a proton beam (**Pb1**) of 80 keV and 30 mA. Such a beam will be further accelerated inside the **RFQ** and emerges form it with and energy of 5 MeV and still 30 mA in current (**Pb2**) for impacting the Beryllium target (**T**) where the neutrons (**n**) are generated based on the previously mentioned $^{9}Be(p,xn)$ reactions. The Beryllium target showed in figure I.1 is one of the two Be-based neutron converter prototypes that have already been designed, constructed and undergone into a series of thermo-mechanical and radiation damage tests

This report concerns Monte Carlo modeling for a Beam Shaping Assembly (BSA), designed to produce an intense thermal neutron beam for skin melanoma treatments. The p+Be neutron production yields used in the calculations have been taken from literature (ref 4.) from 4 MeV proton beam. This choice is due to the lack in the literature of a complete set of neutron spectra at different yielding angles for 5 MeV case. The measurement of such spectra using the CN-LNL Van de Graaff accelerator for 5 MeV protons is one of the project goals.

The neutron source spectra[4] for the p+Be reaction for different angles and a proton beam energy of 4 MeV are showed in figure I.2.

Neutrons are conventionally classified into three energy ranges in BNCT:

Fast neutrons:		E > 10 keV
Epithermal neutrons :	0.5 eV	E < 10 keV
Thermal neutrons :		E < 0.5 eV

For better treating the shallow skin melanoma with BNCT a neutron flux as thermal as possible at the irradiation position is desired. The in-air neutron beam port recommended limits taken into account at the design level for evaluating the quality of such a beam at the irradiation position for the BNCT[5] are reported in table I.1.

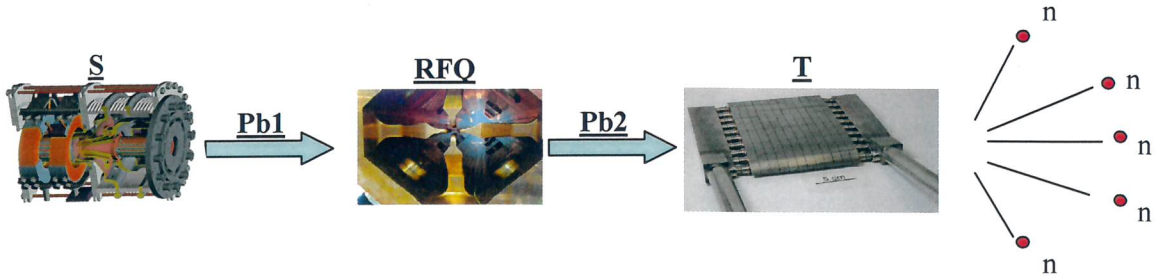

Fig.I.1. Scheme of the neutron production process. S: TRIPS proton source. Pb1: Proton beam of 80 keV, 30 mA. B: RFQ. Pb2: Proton beam of 5 MeV, 30 mA. T: Beryllium target.

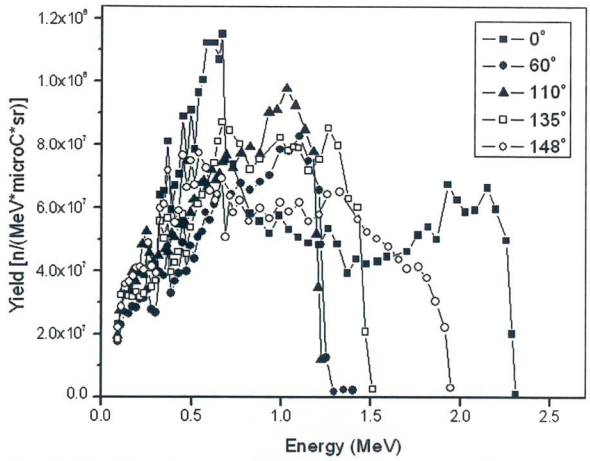

Fig. I.2 Be-9 thick target neutron yield sepectra at 4MeV proton beam

Table I1.BNCT in-air neutron beam port recommended limit.

Parameter	limits
Thermal neutrons flux. ϕ_{th} [n/cm^{2}s]	$\geq 1.10^9$
Thermal to Total neutrons flux ratio. ϕ_{th} / ϕ_{tot}	≥ 0.9
Epithermal plus fast neutrons dose rate to thermal neutrons flux ratio. $\dot{D}_{n,epi+fast} / \phi_{th}$ [Gy cm^2]	$\leq 2*10^{-13}$
Gamma dose rate to thermal neutrons flux ratio. $\dot{D}_{\gamma} / \phi_{th}$ [Gy cm^2]	$\leq 2*10^{-13}$

The neutron spectra from figure I.2 are far away from accomplish the requirements reported in table 1 thus a so a BSA should be used for shifting the neutron spectrum to the desired energy range, while keeping the undesired and unavoidable gamma ray background as low as possible.

The materials usually used for constructing the BSA are commonly classified into three groups:

Spectrum shifter: A material able to slowdown the fast neutrons into the epithermal or thermal region, with limited neutron capture. Commonly used materials are: H_2O, D_2O and BeO.

Filter: A material able to further shift the epithermal neutrons resulting from the moderation process into the desired energy range (in our case the thermal region) with little absorption. The filter material should additionally have a high absorption rate for the remaining "non-moderated" fast neutrons. Among the filter materials it can be found: Fe, Mg and S.

Reflector: A material with a high neutron albedo able to "confine" the neutrons into the BSA geometry by scattering them with low absorption. C and Pb are mostly used for this scope.

At present, there exists a BSA prototype at LNL, designed and tested some years ago.[6] Figure I.3 shows a cutaway view of the facility.

This prototype is mainly composed by a heavy water (D_2O) box, acting as spectrum shifter and a reactor-grade graphite (RG-Graphite) reflector, using no filtering materials at all.

The aim of the present work was to try out some variants of that configuration using the MCNPX (ver2.6b) transport code[7] and see their effect in the resulting neutron flux at the irradiation port, based on the parameters reported in table I.1

II. TARGET EMISSION PROFILE.

Figure II.1 shows the simulated geometry of the "duck beak"-like beryllium neutron converter. The image was generated using the 3D MCNPX geometry plotter Sabrina v4.25.[8] The arrow represents the incoming proton beam (**Pb**).

The MCNPX code, which has been used for the facility design, can perform the transport of a set of charged particles (including protons) in a wide energy range, with a validated accuracy. However, the given ENDF/B-VI library includes evaluated cross sections data for only part of all ^{9}Be(p,xn) nuclear reaction channels which are opened at 5 MeV. Some benchmark calculations performed to predict the neutron spectrum at 0° (i.e. along the beam incoming direction), confirmed, in fact, the need to skip the p-n simulation process. A preliminary approach, using a complete set of available experimental double differential neutron yielding spectra at 4 MeV, has been widely employed instead, due to lack of detailed data at the designed 5 MeV proton energy.

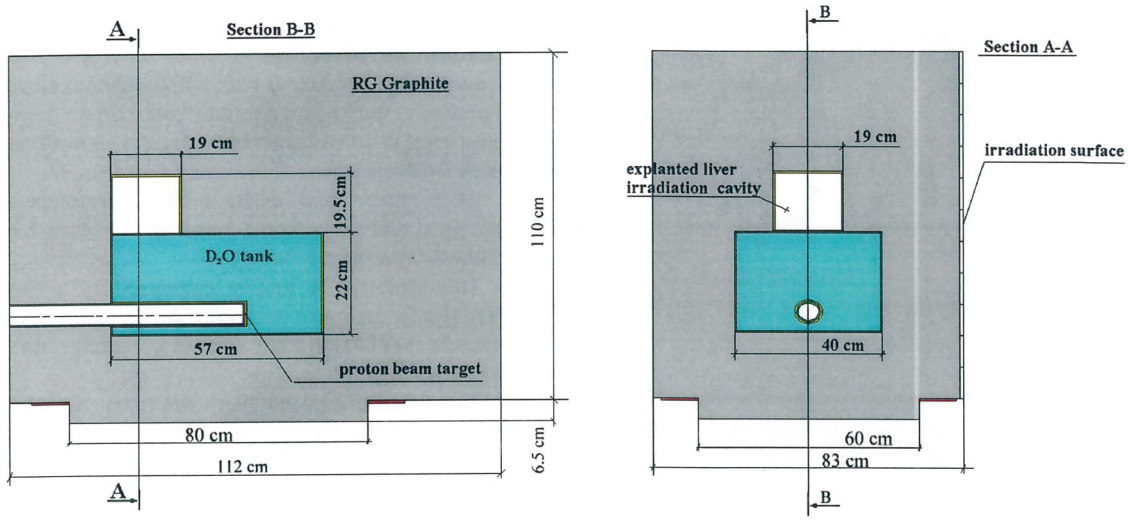

Fig.I.3 Cutaway view of the existing BSA prototype at LNL

Therefore the MCNPX simulations did not include the transport of the protons for the p + Be interactions. Each point of the Beryllium surface was considered as a neutron source instead, with the emission spectra according to the neutron spectra showed in figure I.2.

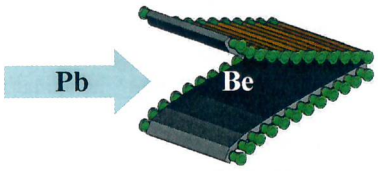

Fig.II.1 MCNP geometry of the Beryllium-made neutron converter. Pb: Proton beam. Be: Beryllium surface

The 3D plot of the neutron emission points showed in figure II.2, confirm that the points follow the profile of the neutron converter.

Furthermore the neutron emission points were generated following the general parabola equation $(X\text{-}Xo)^2 = 2p(Y\text{-}Yo)^2$ for the X-coordinate, while keeping homogeneously distributed the Y and Z-coordinates, like that provided by RFQ accelerator for the incoming proton beam.

Figures II.3a and II.3b show that distribution over one of the source branches for two different plane projections.

III. BSA MODELING: FIRST STAGE.

As it was mentioned in the introduction, the starting configuration for the BSA design was based on an existing prototype showed in figure I.3.

The simulations were based on a MCNP model of the facility that it had been previously validated with experimental measurements.[6] In figure III.1 it is shown a MCNP 2D plot of the geometry.

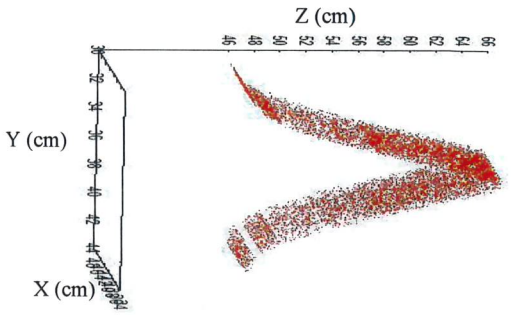

Fig.II.2. Neutrons emission points over the entire source emitting surfaces.

In table III.1 are shown the values of the evaluation parameters mentioned in table I.1, for the original BSA geometry that already exists at LNL. The reference limits for each parameter are highlighted in the first row of the tale. All values are referred to the irradiation position that covers an area of 10 x 10 cm^2.

It can be seen that the only parameter that fulfills the requirements is the thermal neutron flux. But with a

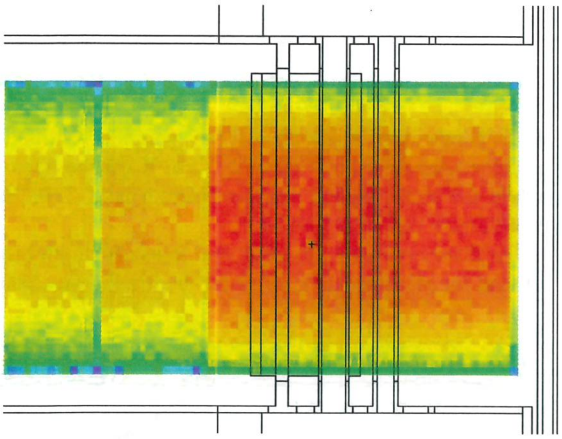

Fig. II.3a. Z-X projection of the neutrons emission points over the source surface for a parabolic distribution.

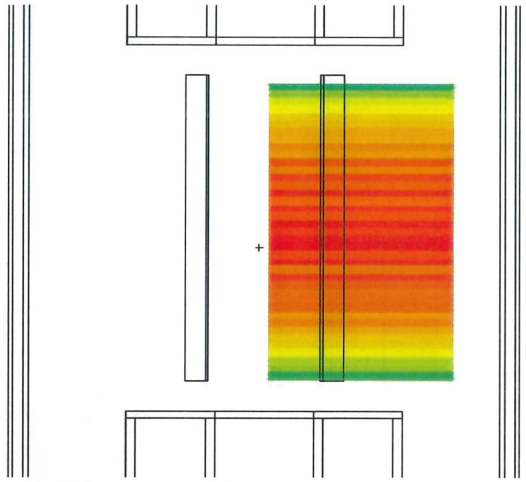

Fig.II.3b. Y-X projection of the neutrons emission points over the source surface for a parabolic distribution.

Table III.1 Value of the evaluation parameters for the original BSA configuration present at LNL .The highlighted values (first row) are the reference limits.

ϕ_{th} (n/cm^{2}s)	$\frac{\phi_{th}}{\phi_{tot}}$	$\frac{\dot{D}_{n(epi+fast)}}{\phi_{th}}$ (Gy·cm^2)	$\frac{\dot{D}_{\gamma}}{\phi_{th}}$ (Gy·cm^2)
> 10^9	**> 0.90**	**< 2 * 10^{-13}**	**< 2 * 10^{-13}**
2.00*10^9	0.79	2.94*10^{-13}	7.89*10^{-13}

thermal neutron flux to total neutron flux spectral ratio of 0.79 this neutron beam is far from being as thermal as needed. Also the other two parameters that reflect the undesired epithermal and fast neutrons dose as well as the gamma dose contributions are out of the accepted limits. The MCNP geometry of the facility is showed in figures III.1a-b.

After studying different configurations of the target surrounding materials, a first stage of the BSA was produced as shown in figure III.2. Table III.2 reflects the values of the evaluation parameters for this configuration (b) compared to the previous one (a).

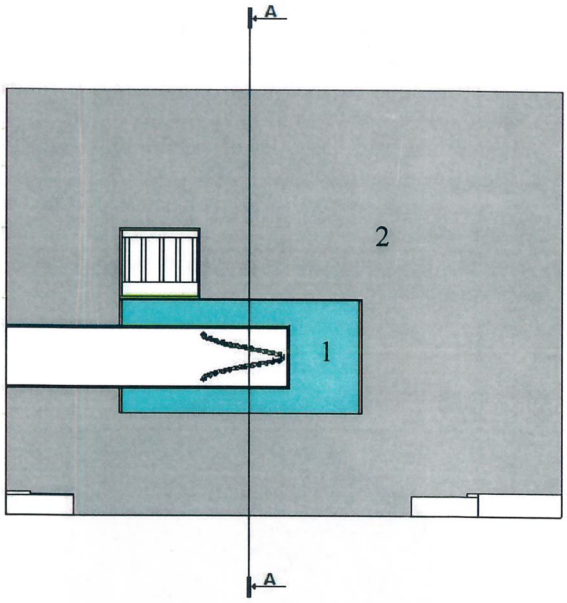

Fig. III.1a MCPX-generated 2D geometry of the BSA facility at LNL.Side View. 1)Heavy water. 2) RG-Graphite.

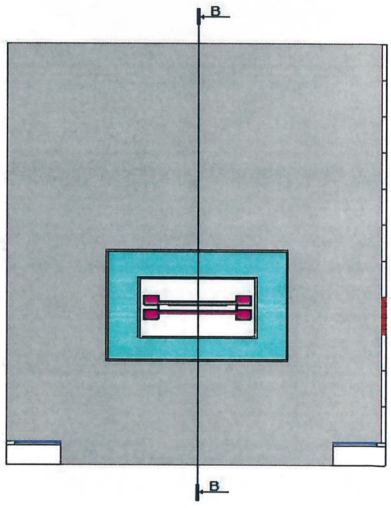

Fig. III.1b MCPX-generated 2D geometry of the BSA facility at LNL. Front View.

It can be seen from the table that although the thermal neutron flux decreases it remains acceptable high, while

the other parameters are improved. Nevertheless thermal spectral ratio is still below 0.9.

In this case the graphite was surrounded by a lead layer of 10 cm of thickness in all sides but the one containing the irradiation port where 11 cm of lead were used. The Pb free volume related to the 10 x 10 cm^2 of the irradiation window was filled with bismuth.

The bismuth was chosen in order to decrease the gamma flux that reaches the irradiation port. Even when bismuth mass attenuation coefficient for gamma rays is similar to that of lead (their atomic numbers differ just by one), bismuth, however, has a lower capture cross section for thermal neutrons. Figures III.3 and III.4 show the interaction cross sections of bismuth and lead from thermal to fast neutron energies. It can be seen that for thermal energies, the capture cross section of lead is more than twice that of bismuth.

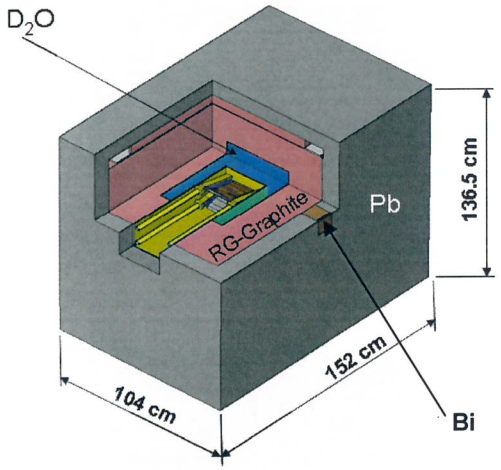

Fig. III.2. First stage of the new BSA configuration

Table III.2 Value of the evaluation parameters for the new BSA configuration (a) and the previous one (b). The highlighted values (first row) are the reference limits.

ϕ_{th} (n/cm²s)	$\frac{\phi_{th}}{\phi_{tot}}$	$\frac{\dot{D}_{n(epi+fast)}}{\phi_{th}}$ (Gy·cm²)	$\frac{\dot{D}_{\gamma}}{\phi_{th}}$ (Gy·cm²)
> 10^9	**> 0.90**	**< 2 * 10^{-13}**	**< 2 * 10^{-13}**
(a) 2.00*10^9	0.79	2.94*10^{-13}	7.89*10^{-13}
(b) 1.55*10^9	0.83	1.89 * 10^{-13}	1.5 *10^{-13}

Also bismuth produces a gamma spectrum from the radiative neutron capture "softer" than that of lead. Figure III.5 shows the spectrum of the gammas emitted by neutron capture from ^{209}Bi and ^{207}Pb. It can be seen that while the more intense line for bismuth is at 319.7 keV, which from lead is at 7367 keV.

For those reasons it was preferred to use Bismuth instead of lead for shielding the gammas at the irradiation channel.

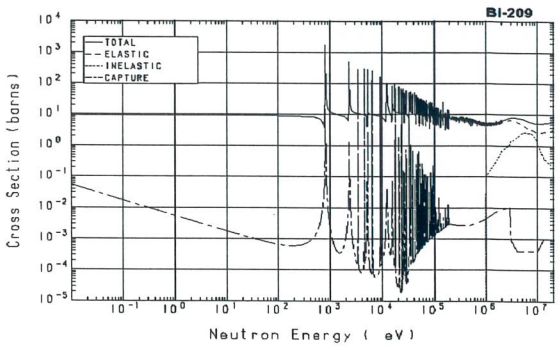

Fig.III.3. Bi-209 neutron interaction cross section (ENDF/B VI)

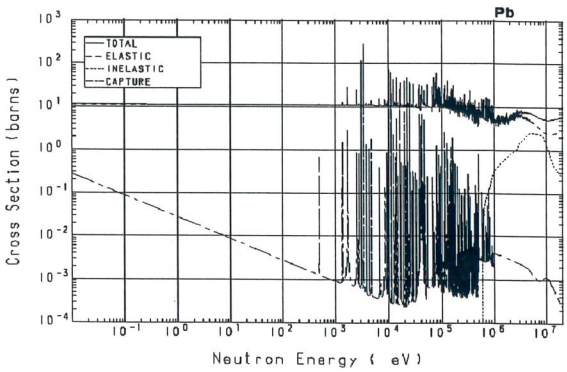

Fig.III.4. Pb neutron interaction cross section (ENDF/B VI)

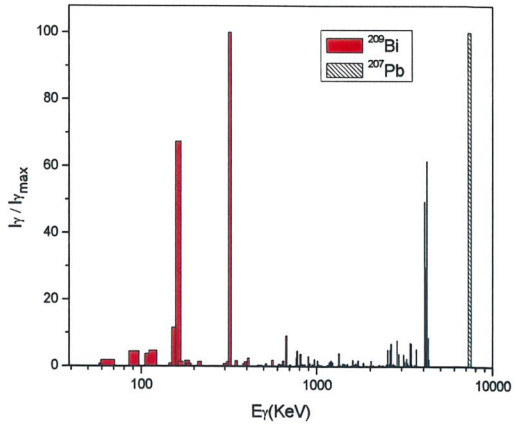

Fig.III.5. Gamma emission spectrum from radiative capture for Bi-209 and Pb-207. (National Nuclear Data Center–Brookhaven National Laboratory. http://www.nndc.bnl.gov/)

IV. BSA MODELING: INTERMEDIATE STAGE.

Starting from the former configuration a series of new computer simulation trials were made, following the principle of keeping as much as possible the original configuration. As a result a new configuration showed in figure IV.1 was produced.

Table IV.1 shows the new calculated values for the evaluation parameters for this new configuration (c) and the previous ones. (a,b)

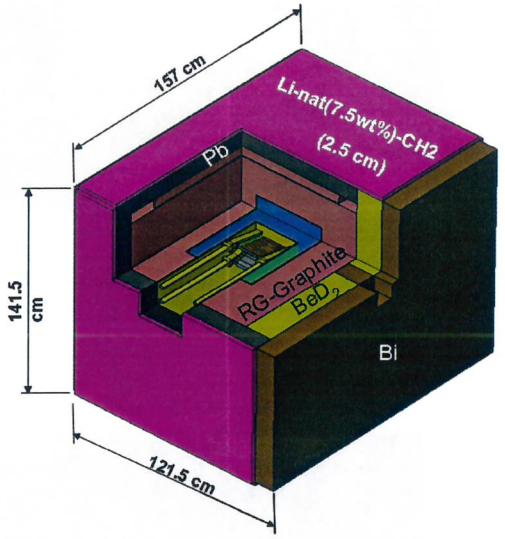

Fig. IV.1. Intermediate stage of the new BSA configuration

Table IV.1 Evaluation parameters calculated values for the new BSA configuration and the previous ones. The highlighted values (first row) are the reference limits.

ϕ_{th} (n/cm^{2}s)	$\frac{\phi_{th}}{\phi_{tot}}$	$\frac{\dot{D}_{n(epi+fast)}}{\phi_{th}}$ (Gy·cm^2)	$\frac{\dot{D}_{\gamma}}{\phi_{th}}$ (Gy·cm^2)
> 10^9	**> 0.90**	**< 2 * 10^{-13}**	**< 2 * 10^{-13}**
(a) 2.00*10^9	0.79	2.94*10^{-13}	7.89*10^{-13}
(b) 1.55*10^9	0.83	1.89 * 10^{-13}	1.5 *10^{-13}
(c) 6.85 *10^8	0.99	7.67 * 10^{-15}	1.08 * 10^{-13}

At this point the thermal neutrons represent the 99% of all neutrons, so the neutron beam at the irradiation position is highly thermal, as it is desired. Also the dose rate parameters, regarding the epithermal plus thermal neutrons and the gammas are improved. The drawback of such a configuration is that the net thermal neutron flux fell below the 10^9 n/cm^{2}s limit.

The main changes of this design consist on the addition of 15 cm of BeD_2 for a further moderation of the neutrons coming from the heavy water tank. Also the lead was substituted by bismuth in the patient-facing wall and a 2.5 cm of Lithiated-Polyethylene (Li-nat(7.5wt% ^{6}Li)-CH_2) layer was added to the rest of the walls for increasing the capture of the thermal neutrons that escape throughout those walls.

The characteristic of the neutron and gamma fluxes not only at the 10 x 10 cm^2 area corresponding to the irradiation position, but along the entire patient-facing wall, was then investigated. For that scope a grid of 2x2 cm^2 pixel size was put in front of the wall and at 10 cm from it as shown in figure IV.2, in order to map in the MCNPX simulations neutrons and gamma dose rate distribution over the wall surface.

Figures IV.3a-b to IV.5a-b show the results for the thermal, epithermal and fast neutrons components of the beam, while figures IV.6a and IV.6b show the result for the gamma radiation. The square on the 2D images represent the 10 x 10 cm^2 irradiation port position.

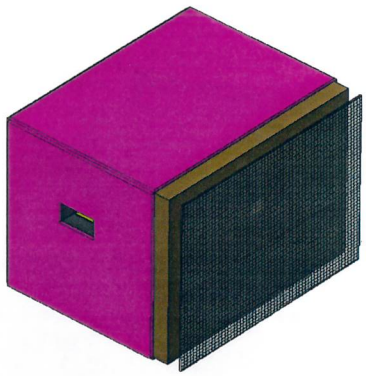

Fig. IV.2. Image of the grid (2x2 cm^2 pixel size) used to map the neutrons and gamma dose rate over the patient-facing wall.

Table IV.2 shows the average dose rate on the *irradiation position* (I.P.) and over the *rest of the wall* (R.W.) for each component of the beam, along with the percent of the total dose rate that corresponds to *the irradiation port area* (I.P.A.).

Table IV.2 Average dose rate on the irradiation position and over the rest of the wall for each component of the beam

Beam component	**I.P.** (Gy/h)	**R.W** (Gy/h)	**I.P.A.** (%)
Thermal neutrons	4.1*10^{-1}	1.3*10^{-1}	76
Epithermal neutrons	1.4*10^{-3}	1.4*10^{-4}	91
Fast neutrons	1.9*10^{-2}	1.3*10^{-3}	94
Gamma	3.6*10^{-1}	6.3*10^{-2}	85

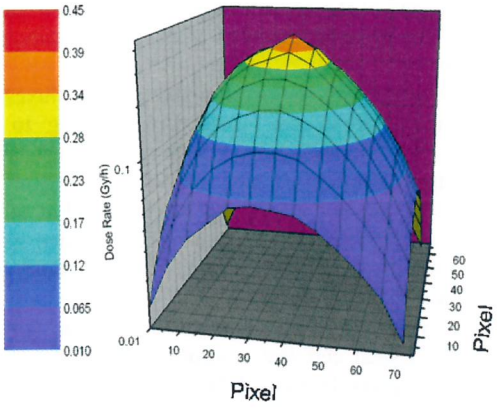

Fig. IV.3a. Plot of the thermal neutrons dose rate [Gy/h] distribution over the patient-facing wall.

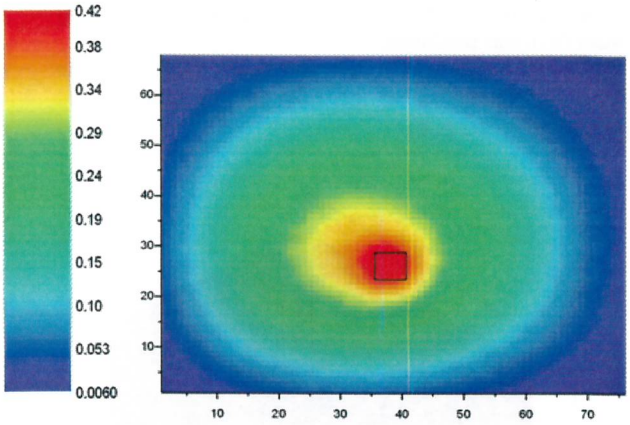

Fig. IV.3b. 2D image of the thermal neutrons dose rate [Gy/h] distribution over the patient-facing wall. The square represents the irradiation port position.

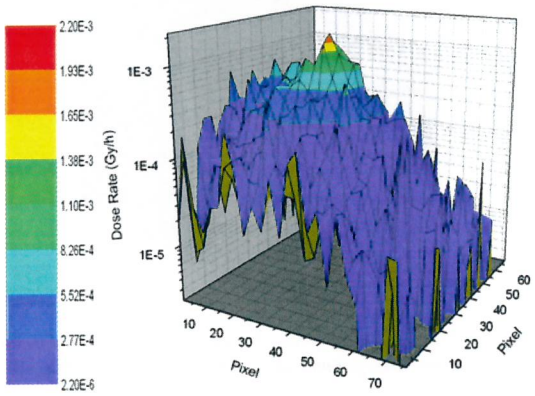

Fig. IV.4a. Plot of the epithermal neutrons dose rate [Gy/h] distribution over the patient-facing wall.

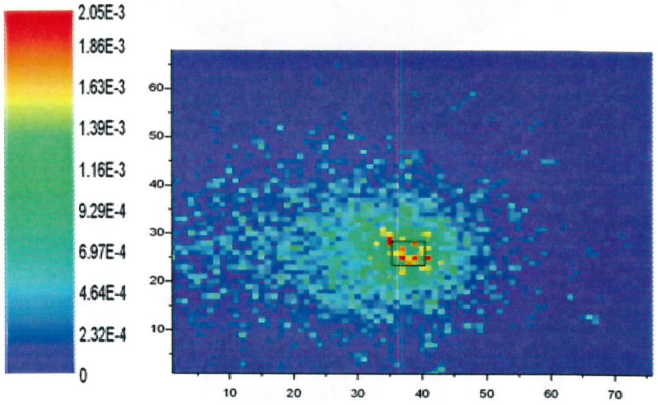

Fig. IV.4b. 2D image of the epithermal neutrons dose rate [Gy/h] distribution over the patient-facing wall. The square represents the irradiation port position.

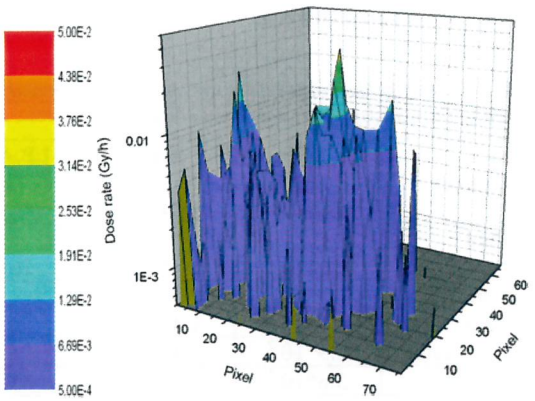

Fig. IV.5a. Plot of the fast neutrons dose rate [Gy/h] distribution over the patient-facing wall.

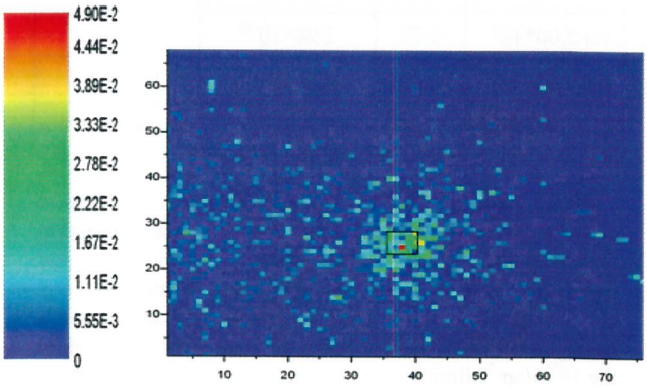

Fig. IV.5b. 2D image of the fast neutrons dose rate [Gy/h] distribution over the patient-facing wall. The square represents the irradiation port position.

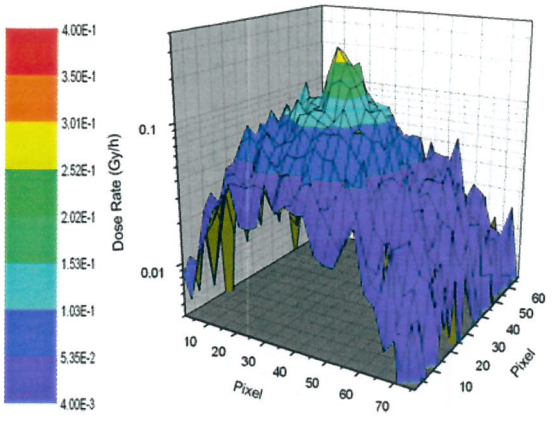

Fig. IV.6a. Plot of the gamma dose rate [Gy/h] distribution over the patient-facing wall.

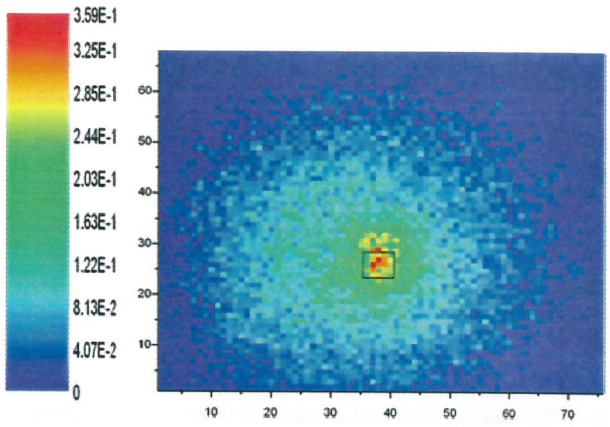

Fig. IV.6b. 2D image of the gamma dose rate [Gy/h] distribution over the patient-facing wall. The square represents the irradiation port position.

It can be seen from table IV.2 and the related figures that the beam is not well collimated on the irradiation port, especially for the thermal neutrons where only 76% of the total dose rate corresponds to the irradiation position. This means that during a patient irradiation session, the total body dose would be high and consequently also the damage to the healthy tissue.

V. BSA MODELING: FINAL STAGE

The results obtained so far from the latest BSA configuration, show that all the evaluation parameters except for the thermal neutron flux accomplish the established reference limits (see table IV.1). Anyway there is a poor collimation of the beam on the irradiation port. Therefore it was decided to abandon the constrain of designing the BSA by just making small change to the original configuration existing at LNL.

A lot of parametric studies were made concerning the geometry and the elemental composition of every component of the BSA and their influence on the moderation, absorption and collimation of the neutrons on their path to the irradiation position. As a result, the final geometry configuration was produced, as shown in figure V.1 shows that configuration.

On more time the value of the evaluation parameters for this new configuration (d) are compared to the previous ones (a-c) as shown in table V.1.

With this final configuration the thermal neutron flux at the irradiation position surpasses the minimum established threshold of 10^9 n/cm^{2}s, while the rest of the parameters fulfill the requirements for BNCT treatment of the shallow skin melanoma treatment.

The main characteristic of this final configuration are the enlargement of heavy water tank, especially towards the irradiation port for improving the moderation of the neutrons, the substitution of the graphite for beryllium oxide (BeO) in order to exploit its remarkable albedo property for better confining and moderating the neutrons inside the BSA volume. Another important improvement was the use of a 2.5 cm layer of lithium fluoride (LiF) covering five out of the six walls of the BSA for absorbing the thermal neutrons that escape throughout those walls, based on the $^6\mathrm{Li}(\mathrm{n}, {}^4_2He)^3_1H$ reaction. Since the LiF is hydrogen free, it has an advantage over the Li-nat(7.5wt%)-CH_2. The presence of hydrogen on the later increases the gamma background due to the $^1_1H\ (\mathrm{n},\gamma)^2_1H$ (radiative capture) reaction.

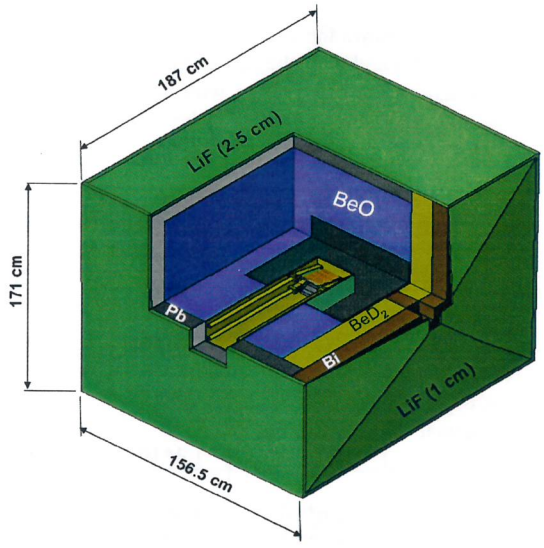

Fig. V.1. Final stage of the new BSA configuration.

Another important feature of this configuration is the use of a 5 cm high-truncated pyramid-like LiF collimator of 1 cm thickness over the patient-facing wall.

Also in this case, a grid of 2x2 cm^2 pixel size was put in

front of the wall for mapping the neutrons and gamma dose rate distribution over the wall

Figures V.4a-b to V.6a-b show the results for the thermal, epithermal and fast neutrons components of the beam, while figures V.7a and V.7b show the result for the gamma radiation. The square on the 2D images represent the 10 x 10 cm^2 irradiation port position.

Table V.1 Calculated values of the evaluation parameters for the final BSA configuration and the previous ones. The highlighted values (first row) are the reference limits.

ϕ_{th} (n/cm^{2}s)	$\frac{\phi_{th}}{\phi_{tot}}$	$\frac{\dot{D}_{n(epi+fast)}}{\phi_{th}}$ (Gy·cm^2)	$\frac{\dot{D}_{\gamma}}{\phi_{th}}$ (Gy·cm^2)
> 10^9	**> 0.90**	**< 2 * 10^{-13}**	**< 2 * 10^{-13}**
(a)2.00*10^9	0.79	2.94*10^{-13}	7.89*10^{-13}
(b)1.55 *10^9	0.83	1.89 * 10^{-13}	1.5 *10^{-13}
(c)6.85 *10^8	0.99	7.67 * 10^{-15}	1.08 * 10^{-13}
(d)1.17*10^9	0.99	7.93*10^{-16}	1.37*10^{-13}

Table V.2 shows the average dose rate on the irradiation position (I.P.) and over the rest of the wall (R.W.) for each component of the beam along with the percent of the total dose rate that corresponds to the irradiation port area (I.P.A.).

Table V.2 Average dose rate on the irradiation position and over the rest of the wall for each component of the beam.

Beam component	**I.P.** (Gy/h)	**R.W** (Gy/h)	**I.P.A.** (%)
Thermal neutrons	7.0*10^{-1}	1.9*10^{-3}	99.7
Epithermal neutrons	6.8*10^{-4}	1.4*10^{-5}	98
Fast neutrons	2.6*10^{-3}	8.3*10^{-5}	97
Gamma	5.8*10^{-1}	5.3*10^{-2}	92

It can be seen from table V.2 and the related figures that for this last configuration, the neutron beam is very well collimated on the irradiation port. The less collimated component of the beam is the gamma radiation, because those gammas are mainly produced by radiative capture of thermal neutrons inside the BSA volume and thermal neutrons diffuse stochastically inside the BSA. Nevertheless 92 % of the gammas come out through the irradiation port.

Figure V.2 shows the neutron fluence rate per lethargy unit ($cm^{-2}s^{-1}u^{-1}$) while figure V.7 show the neutron kerma rate (Gy/min). In both cases the spectra for the irradiation position (dotted line) and the rest of the wall (straight line) are reported

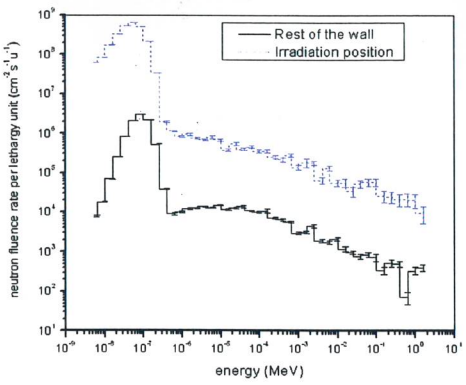

Fig. V.2. Neutron fluency rate per lethargy unit spectra for irradiation position (dotted line) and the rest of the wall (straight line)

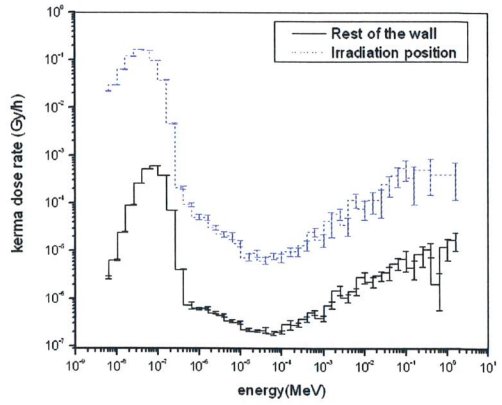

Fig. V.3. Neutron kerma dose rate spectra for irradiation position (dotted line) and the rest of the wall ((straight line)

Figure V.3 reveals the importance of reducing as much as possible the fast neutrons component of the beam (En > 10 keV), since even very low values of neutron fluency for that energy region (fig. V.2) represent an important contribution in terms of dose rate.

For an integral characterization of the facility, the average dose rate for neutrons and gammas for each wall was calculated. Figure V.8 shows the convention followed for naming the walls. The results are reported in figure V.9 and table V.3 (Th.N-*Thermal Neutrons*; Epi.N-*Epithermal Neutrons*; F.N.-*Fast Neutrons*; G-*Gamma.*)

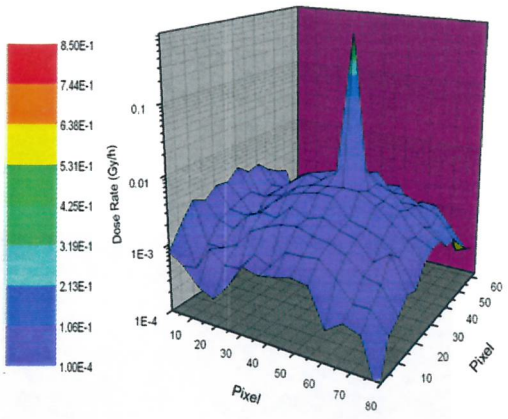

Fig. V.4a. Plot of the thermal neutrons dose rate [Gy/h] distribution over the patient-facing wall.

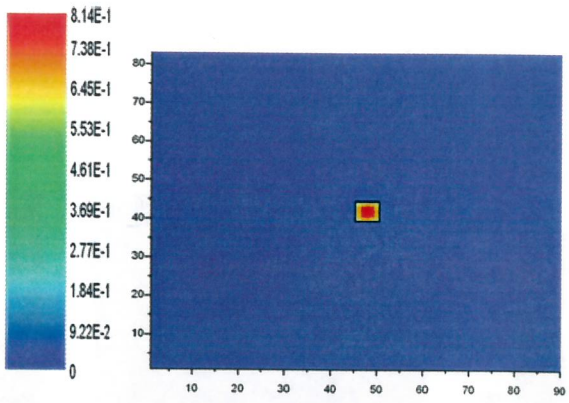

Fig. V.4b. 2D image of the thermal neutrons dose rate [Gy/h] distribution over the patient-facing wall. The square represents the irradiation port position.

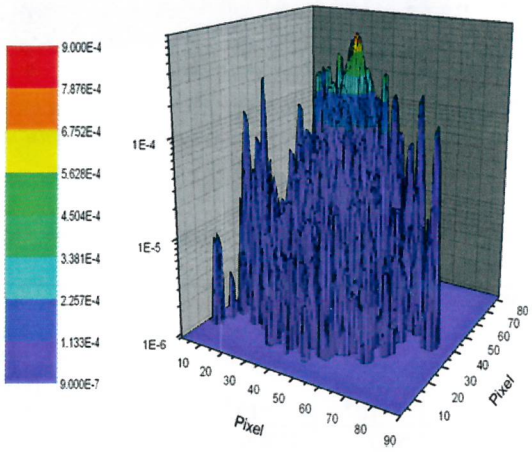

Fig. V.5a. Plot of the epithermal neutrons dose rate [Gy/h] distribution over the patient-facing wall.

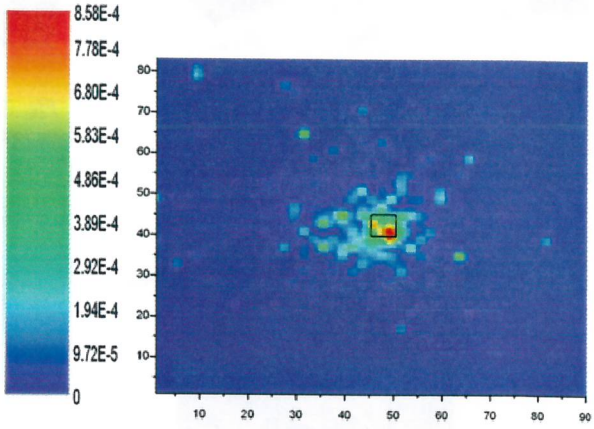

Fig. V.5b. 2D image of the epithermal neutrons dose rate [Gy/h] distribution over the patient-facing wall. The square represents the irradiation port position.

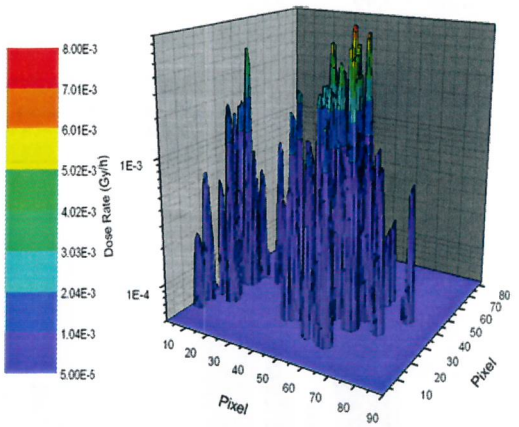

Fig. V.6a. Plot of the fast neutrons dose rate [Gy/h] distribution over the patient-facing wall.

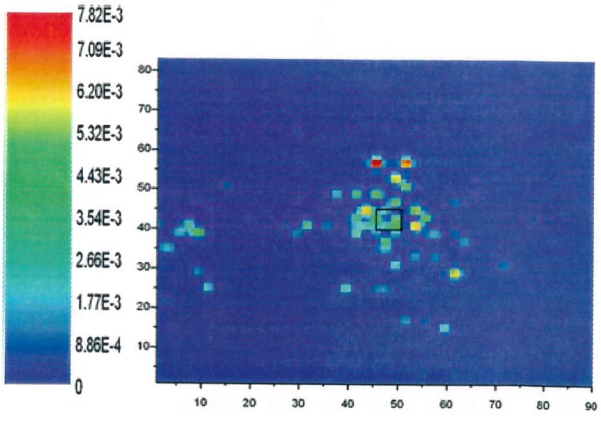

Fig. V.6b. 2D image of the fast neutrons dose rate [Gy/h] distribution over the patient-facing wall. The square represents the irradiation port position.

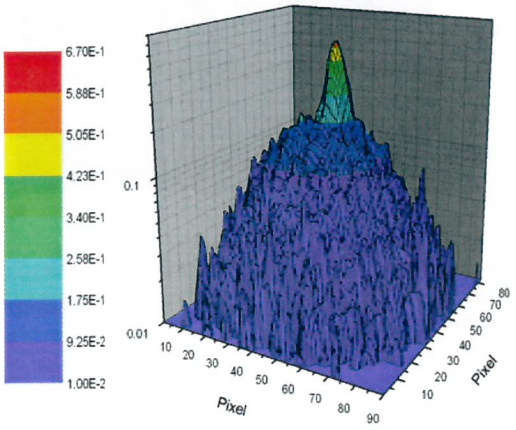

Fig. V.7a. Plot of the gamma dose rate [Gy/h] distribution over the patient-facing wall.

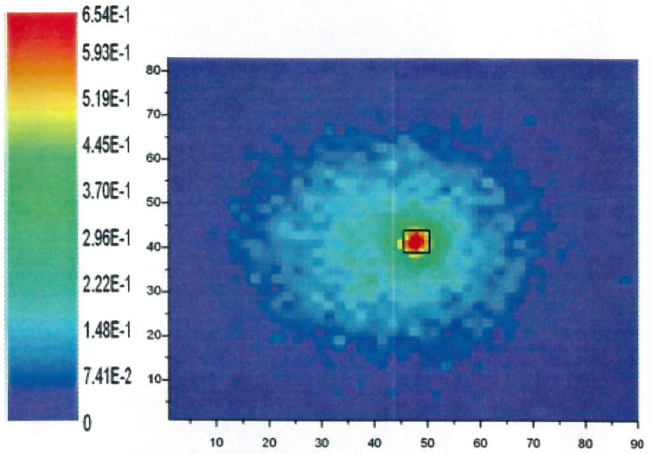

Fig. V.7b. 2D image of the gamma dose rate [Gy/h] distribution over the patient-facing wall. The square represents the irradiation port position.

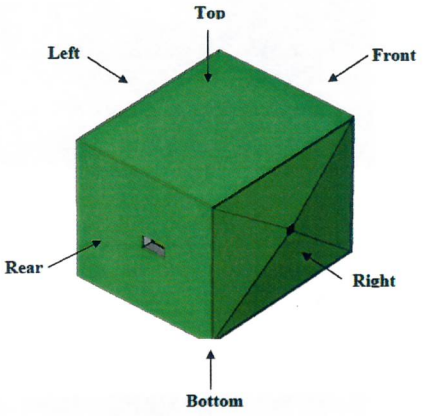

Fig.V.8. Naming convention used for characterizing the facility according to the average dose rates of neutron and gamma radiation.

Regarding the neutron components, the "rear" wall presents the higher values because on their path to that wall, the neutrons traverse the vacuum volume of the proton beam pipe, so they are under moderated.

The second important contribution is "right" wall that in this case does not include the irradiation port region. Here the main role for the neutron dose rate is played by the thermal neutrons while the fast neutron component is highly depressed.

For the rest of the walls the neutron dose rate is very low.

In the case of the gamma radiation, for all walls the dose rate is still high, of the order of tenths of mGy/h. This problem may be solved by increasing the shielding for gamma radiation, using supplementary layers of lead or bismuth.

Table V.3 Average dose rate for neutron and gamma radiation for each wall of the BSA

Wall	Th. N. dose rate (Gy/h) $*10^{-6}$	Epi. N. dose rate (Gy/h) $*10^{-8}$	F. N. dose rate (Gy/h) $*10^{-6}$	G. dose rate (Gy/h) $*10^{-2}$
Rear	5.81	41800	145000	5.97
Front	3.03	18.5	3.26	6.53
Right	1930	1430	88.7	5.26
Left	3.9	0	0	4.49
Bottom	4.49	28.2	0	8.61
Top	4.88	1.09	0	8.57

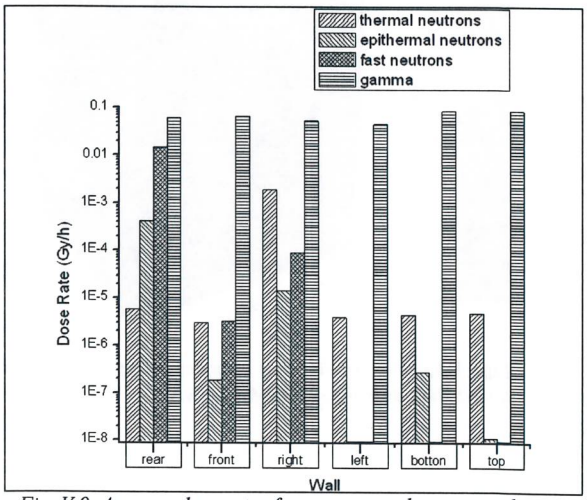

Fig. V.9. Average dose rates for neutron and gamma radiation for each wall of the BSA.

VI. CONCLUSIONS.

The present MCNPX design of the proposed irradiation facility, based on 4 MeV proton neutron yields, is be able to provide a high collimated thermal neutron beam (99.7 %), fulfilling all the established reference parameters for a BNCT irradiation facility

Further improvements shall be made for better shielding the gamma radiation, like using supplementary layers of lead or bismuth.

An experimental project is planned by LNL to measure neutron yields of the $p(^{9}Be, n)^{9}B$ using a thick target and 5 MeV proton beams. Neutron yields will be measured from 0° to 135°. When the whole set of Be neutron yielding spectra at the operative 5 MeV energy will be available, the actual model will be implemented with. Because neutron yields at 5 MeV are higher than those ones at 4 MeV, the final thermal-neutron irradiation-facility performance is expected to be better than performance presented in this report.

References.

1. A. Pisent, P. Colautti, J. Esposito, L. De Nardo, V. Conte, S. Agosteo, G. Jori, P.A. Posocco, L.B.Tecchio, R.Tinti, G. Rosi *Progress on the accelerator based SPES-BNCT project at INFN Legnaro IOP online journal:* Journal of Physics Conference Series 41, (2006) 391-399;

2. G.L. Locker, *Biological effets and therapeutic possibilities of neutrons,* Am Roentgenol. 36 (1936), 1-13

3. E. Fagotti et al. *First Beam of SPES Source at LNL.* LNL Annual Report (2006) 192-193

4. W.B. Howard, S.M. Grimes, S.I. Al Quarinshi, D. K. Jacobs, C.E. Brient J.C. Yanch, *Measurement of the thick target 9-Be(p,n) Neutron Energy Spectra.* Nuclear Science Engineering, 138, 145-160 (2001)

5. Current Status of BNCT. IAEA-TECDOC-1223. IAEA. May 2001

6. S. Agosteo, G. Bodei, P. Colautti, et. al. *An accelerator based thermal neutron source for BNCT* Advances in Neutron Capture Therapy, Volume , Medicine and Physics. Elsevier Science B.V., 1997

7. J.S.Hendricks. *MCNPX, VERSION 2.6.A*, LA-UR-05-8225, October 24, 2005.

8. K. A. Van Riper. *Sabrina User's Guide copyright 1997-2005*, White Rock Science.